Optimal Control Laws for Heliocentric Transfers with a Magnetic Sail

Alessandro A. Quarta *, Giovanni Mengali, Generoso Aliasi

Department of Civil and Industrial Engineering, University of Pisa, I-56122 Pisa, Italy

Abstract

A magnetic sail is an advanced propellantless propulsion system that uses the interaction between the solar wind and an artificial magnetic field generated by the spacecraft, to produce a propulsive thrust in interplanetary space. The aim of this paper is to collect the available experimental data, and the simulation results, to develop a simplified mathematical model that describes the propulsive acceleration of a magnetic sail, in an analytical form, for mission analysis purposes. Such a mathematical model is then used for estimating the performance of a magnetic sail-based spacecraft in a two-dimensional, minimum time, deep space mission scenario. In particular, optimal and locally-optimal steering laws are derived using an indirect approach. The obtained results are then applied to a mission analysis involving both an optimal Earth-Venus (circle-to-circle) interplanetary transfer, and a locally-optimal Solar System escape trajectory. For example, assuming a characteristic acceleration of $1\,\mathrm{mm/s^2}$, an optimal Earth-Venus transfer may be completed within about 380 days.

Key words: Magnetic sail, Trajectory Optimization, Solar System escape

* Corresponding author.
Email addresses: a.quarta@ing.unipi.it (Alessandro A. Quarta), g.mengali@ing.unipi.it (Giovanni Mengali), g.aliasi@dia.unipi.it (Generoso Aliasi).

Nomenclature

a	=	semimajor axis of osculating orbit
$\boldsymbol{a}$	=	propulsive acceleration, see Eq. (1)
a_c	=	spacecraft characteristic acceleration
C_D	=	drag coefficient
C_L	=	lift coefficient
$\mathcal{E}$	=	specific mechanical energy
h_0, h_1, k_0, k_1	=	best fit coefficients, see Eqs. (2)-(3)
H	=	Hamiltonian function
$\hat{\boldsymbol{\imath}}_r$	=	unit vector in the radial direction
$\hat{\boldsymbol{\imath}}_\nu$	=	unit vector in the transverse direction
J	=	performance index
$\boldsymbol{M}$	=	magnetic dipole vector
$\boldsymbol{p}$	=	reference vector (with $p \triangleq \|p\|$)
r	=	Sun-spacecraft distance (with $r_\oplus \triangleq 1\,\mathrm{AU}$)
s_f	=	switching function, see Eq. (5)
t	=	time
$\mathcal{T}_\odot$	=	heliocentric polar reference frame, see Fig. 2
u	=	radial component of velocity
v	=	circumferential component of velocity
δ	=	pitch angle of vector $\boldsymbol{p}$
η	=	thrust coefficient, see Eq. (1)
λ	=	adjoint variable
$\mu_\odot$	=	Sun's gravitational parameter
ν	=	polar angle, see Fig. 2

ϕ = thrust angle, see Fig. 2

τ = switching parameter

θ = sail angle of attack, see Fig. 2

Subscripts

0 = initial, parking orbit

1 = final, target orbit

Superscripts

$\sim$ = critical

$'$ = reduced

$\cdot$ = time derivative

$\wedge$ = unit vector

1 Introduction

A magnetic sail (Magsail) is an advanced propellantless propulsion concept that was originally proposed by Andrews and Zubrin [1,2,3,4,5] more than twenty years ago. A Magsail-based spacecraft is essentially constituted by a large loop of conducting material carrying a current, with a few shroud lines that are used to couple the loop with the payload, see Fig 1. The artificial magnetic field generated by the current deflects the charged particles from the solar wind thus producing, in the interplanetary space, a propulsive thrust that is nearly aligned along the Sun-spacecraft direction. A transverse thrust component, albeit of modest magnitude,

can also be obtained by inclining the sail's reference plane (that is, the plane of the large loop). A Magsail is currently a rather exotic propulsion system, because of the technical challenges related to the practical feasibility of such a very large space structure. Indeed, in the original solution proposed by Zubrin and Andrews [4] the loop radius could (theoretically) range from some tens of kilometers up to some hundred kilometers, depending on the thrust level to be obtained.

The Magsail concept has also inspired alternative solutions for exploiting the solar wind as a means to create other kinds of propellantless propulsion systems. Two of the most interesting solutions are the Mini-Magnetospheric Plasma Propulsion (M2P2), proposed by Winglee [6,7], and the Electric Solar Wind Sail (E-sail) invented by Janhunen [8,9]. It is worth noting that the theoretical model discussed by Andrews and Zubrin [1] has been confirmed in recent years by a number of numerical simulations and experimental results, in which different scale models of a Magsail have been investigated [10,11,12,13,14,15,16,17]. The results of these studies give important information on the propulsion system performance in terms of the main design parameters as, for instance, the loop radius.

In this context, the aim of this paper is twofold. On one side the available Magsail experimental data are collected and translated into a mathematical thrust model, suitable for a preliminary mission design in a two-dimensional framework. The second aim is to employ the thrust model for optimizing the Magsail-based spacecraft performance in a deep space mission scenario, in which both the planet's gravitational attraction and the size of the planetary magnetosphere are neglected. The analysis described in this paper complements a similar study on optimal space missions for spacecraft equipped with advanced propulsion systems based either on an M2P2 [18,19], or on an E-sail [20,21,22]. In particular, the succeeding control laws for truly-optimal and locally-optimal deep space trajectories are obtained in a closed-form solution. These control laws are then applied in the analysis of a two-dimensional Earth-Venus interplanetary transfer, and for a Solar System escape mission.

2 Propulsive Acceleration Model

For mathematical purposes it is useful to introduce a heliocentric polar reference frame $\mathcal{T}_{\odot}(r, \nu)$, of unit vectors $\hat{\boldsymbol{i}}_r$ and $\hat{\boldsymbol{i}}_\nu$, where ν is the spacecraft polar angle measured counterclockwise from a fixed direction, while r is the Sun-spacecraft distance. With reference to Fig. 2, the orientation of the magnetic dipole moment vector $\hat{\boldsymbol{M}} \triangleq \boldsymbol{M}/\left\|\boldsymbol{M}\right\|$, which is approximately orthogonal to the sail's reference plane, is univocally defined by the so called angle of attack θ. Figure 2 also shows the thrust angle $\phi \in [-\pi/2,\, \pi/2]$, that is, the angle between the propulsive acceleration vector $\boldsymbol{a}$ and the radial direction $\hat{\boldsymbol{i}}_r$. Note that, in general, $\theta \neq \phi$.

The theoretical analysis by Zubrin and Andrews [4], and the results obtained from numerical simulation and experimental tests on scale models [16,17], have shown that the propulsive thrust of a Magsail system may be expressed as a function of r and θ. However, the solar wind and the sail's magnetic field interact each other in a rather complex way. An accurate mathematical model is therefore difficult to obtain. To simplify the analysis, two limiting cases (or operation modes) are usually considered in the literature [23] depending on the size of the Magsail's magnetic cavity. The first case, referred to as "case A", corresponds to a very large Magsail with a loop radius on the order of some hundreds kilometers. The second case, or "case B", corresponds to a smaller Magsail, with a loop radius on the order of some kilometers [10,16]. According to Kojima et al. [23], case A is consistent with the so called "thin magnetopause mode", whereas case B refers to the "thick magnetopause mode", see Fig. 3 of Ref. [23].

The performance of a Magsail-based spacecraft can be suitably described as a function of the characteristic acceleration a_c. The latter, in analogy to the nomenclature adopted for a photonic solar sail [24,25,26], is defined as the maximum propulsive acceleration at a reference Sun-spacecraft distance of $r_{\oplus} \triangleq 1\,\mathrm{AU}$. Bearing in mind the definition of a_c, and taking into account the results of the experimental tests, the Magsail propulsive acceleration $\boldsymbol{a}$ may be

written as

$$\boldsymbol{a} = \tau\, a_c \left(\frac{r_\oplus}{r}\right)^\eta \left(C_D(\theta)\,\hat{\boldsymbol{i}}_r + C_L(\theta)\,\hat{\boldsymbol{i}}_\nu\right) \tag{1}$$

where η is the thrust coefficient ($\eta = 2$ for case A, $\eta = 4/3$ for case B), whereas $\tau = \{0, 1\}$ is the switching parameter that models the Magsail on/off condition and is introduced to account for the presence of coasting arcs in the spacecraft deep space trajectory. Note that the selected value of the thrust coefficient η is consistent with the analytical results of Zubrin and Andrews [4] and Kajimura et al. [16], assuming that the solar wind density varies as $1/r^2$ (see for example Eqs. (1) and (2) of Ref. [16], and Eqs. (3) and (11) of Ref. [4]).

The propulsive thrust may be theoretically switched off by setting the current within the loop to zero. However, such an event must be considered with care for problems related to possible electric power deficiency. The reason is that in the original concept by Zubrin and Andrews [4] the large loop constituting the Magsail is made of superconducting material. As a result, once the propulsion system is switched on (at the beginning of the mission), the required current in the loop can be maintained with a modest power consumption. Nonetheless, assuming that the electric power is provided by solar panels, if the current is zeroed at a distance $r \gg r_\oplus$ to get a coasting arc, the power necessary for a succeeding thrust restart could not be available onboard (recall that the solar panels available power roughly scales proportional to $1/r^2$).

Returning to Eq. (1), the dimensionless coefficients C_D and C_L are usually referred to as drag and lift coefficient [17], in analogy to the nomenclature adopted for atmospheric flight mechanics problems. The drag coefficient C_D models the component of the propulsive acceleration in the radial direction, that is, in the (nominal) propagation direction of the solar wind. Note that C_D is strictly positive, that is, the radial thrust is always directed away from the Sun. On the other hand the lift coefficient C_L, which models the transverse thrust component, may take a negative value, meaning that $\boldsymbol{a} \cdot \hat{\boldsymbol{i}}_\nu$ may be less than zero.

In other words, a Magsail-based spacecraft is able to change the angular momentum of the

osculating orbit. However, the presence of a transverse thrust component requires the capability of rotating the sail's reference plane. In principle this is possible by displacing the center of mass of the Magsail with respect to its center of pressure. Even though such a solution may be difficult to accomplish due to the large dimension of the loop radius, it has been theoretically discussed by Zubrin and Andrews [4].

Numerical simulations and experimental tests [16,17] show that the drag and lift coefficients are both functions of θ. However, the relationships $C_D = C_D(\theta)$ and $C_L = C_L(\theta)$ present different behaviors according to whether the Magsail falls within case A or case B. This is clearly illustrated in Fig. 3, which has been obtained using the numerical data taken from Ref. [16]. Note that unlike Ref. [16], in which the radial and transverse thrust components are given in the range $\theta \in [0,\, \pi/2]$, Fig. 3 extends the variation range of θ to the interval $[0,\, \pi]$. This is possible by taking into account the symmetry properties of the drag and lift coefficients [17]. In fact, it may be shown that $C_D(\theta + \pi/2) = C_D(-\theta + \pi/2)$, whereas $C_L(\theta + \pi/2) = -C_L(-\theta + \pi/2)$, as is confirmed by numerical simulations [27]. Also note that the coefficients C_D and C_L of Fig. 3 have been normalized with the maximum value of the drag coefficient. Accordingly, the maximum value of C_D in Fig. 3 is unitary, while the actual maximum value of C_D is directly accounted for in the value of the characteristic acceleration a_c.

The numerical/experimental data (black squares and triangles of Fig. 3) may be described with the following analytical relationships

$$C_D = h_0 + h_1 \cos(2\,\theta) \tag{2}$$

$$C_L = k_0 \sin(2\,\theta) + k_1 \sin(4\,\theta) \tag{3}$$

where the best fit coefficients h_0, h_1, k_0, and k_1 are all given in Table 1. Equations (2) and (3) are useful for the analysis of the optimal control law to be discussed next, and are drawn in Fig. 3 in solid line.

Note that the magnitude of the transverse component of the propulsive acceleration ($\boldsymbol{a} \cdot \hat{\boldsymbol{i}}_\nu$) is anyway much smaller than the radial component ($\boldsymbol{a} \cdot \hat{\boldsymbol{i}}_r$) . This is clearly illustrated in Fig. 4, which compares the two propulsive acceleration components for case A and case B. The solid line represents the locus of points along which the vector endpoint of the normalized propulsive acceleration is constrained to lie when the Sun-spacecraft distance is 1 AU. For the sake of comparison the figure also shows the normalized propulsive acceleration, at the same Sun-spacecraft distance, for a perfectly reflecting photonic solar sail [28,29] and an E-sail. It is worth noting that the thrust angle ϕ for a Magsail does not exceed about 12 deg, while the same thrust angle for an E-sail [30] may reach up to 30 deg.

3 Optimal Control Laws

The aim of this section is to find the optimal control laws of a Magsail for two different mission applications. The first one consists of the solution of a minimum time transfer trajectory in a two-dimensional heliocentric mission scenario. The solution of this problem is useful for the analysis of interplanetary transfers or for estimating the minimum time necessary to reach a given distance from the Sun. The second problem is to find the control law that maximizes the instantaneous rate of change of the specific mechanical energy of a spacecraft in interplanetary space. The latter problem may be used for the study of a direct trajectory for a locally-optimal Solar System escape. With minor adjustments the same control law can also be applied to the analysis of locally-optimal escape trajectories from a planetary gravitational field [5]. Note however that in a planetocentric mission the Magsail would work within the Earth's magnetosphere and the corresponding thrust would be obtained by exploiting the planet's magnetic field rather than the solar wind [5].

It will be shown in the next section that the two previous problems can both be addressed using the same control law type. To that end it is useful to solve the following auxiliary problem:

Given a prescribed vector $\boldsymbol{p}$ belonging to the orbital plane, find the control variables τ and θ such that the projection of $\boldsymbol{a}$ along $\boldsymbol{p}$ is maximized. The latter problem may be solved as follows. Let $\delta \in [-\pi, \pi]$ be the angle between $\boldsymbol{p}$ and the radial direction, such that

$$\boldsymbol{p} = p \left(\cos\delta \, \hat{\boldsymbol{i}}_r + \sin\delta \, \hat{\boldsymbol{i}}_\nu \right) \tag{4}$$

where $p \triangleq \|\boldsymbol{p}\|$ with $p \neq 0$. From Eq. (1), the projection of $\boldsymbol{a}$ along $\boldsymbol{p}$ is

$$\boldsymbol{a} \cdot \boldsymbol{p} = \tau \, p \, a_c \left(\frac{r_\oplus}{r} \right)^\eta s_f \qquad \text{with} \qquad s_f \triangleq C_D \, \cos\delta + C_L \, \sin\delta \tag{5}$$

Substituting the analytical relationships (2) and (3) into Eq. (5), s_f may be written as a function of δ and θ as

$$s_f = [h_0 + h_1 \, \cos(2\,\theta)] \, \cos\delta + [k_0 \, \sin(2\,\theta) + k_1 \, \sin(4\,\theta)] \, \sin\delta \tag{6}$$

Because $\boldsymbol{a} \cdot \boldsymbol{p}$ depends linearly on τ, a bang-bang control law is optimal, that is

$$\tau = \begin{cases} 0 & \text{if} \quad s_f < 0 \\ \\ 1 & \text{if} \quad s_f > 0 \end{cases} \tag{7}$$

where s_f is given by Eq. (6). The presence of a coasting phase in the trajectory, corresponding to $\tau = 0$, is related to the instantaneous value of s_f, which therefore plays the role of a switching function.

From Eq. (5) the maximization of $\boldsymbol{a} \cdot \boldsymbol{p}$ requires the maximization of s_f with respect to θ. The solution is illustrated in Fig. 5, in which the optimal values of θ are drawn as a function of δ for both cases A and B. The same figure also shows the two shaded zones in which a coasting phase occurs. In particular, the optimal thrust is different from zero (that is, $\tau = 1$) when $-\widetilde{\delta} < \delta < \widetilde{\delta}$, where $\widetilde{\delta} \simeq 100.5\,\text{deg}$ for case A, and $\widetilde{\delta} \simeq 101.5\,\text{deg}$ for case B.

There exists also a closed form solution for case A. In fact, because $k_1 = 0$ (see Table 1), the

maximization of s_f with respect to θ is simple to obtain. The result is

$$\theta = \frac{1}{2} \arctan\left(\frac{k_0}{h_1} \tan\delta\right) \qquad \text{for case } A \tag{8}$$

which is in agreement with the curve drawn in Fig. 5(a).

Having found how to maximize $\boldsymbol{a} \cdot \boldsymbol{p}$, it is now possible to address the previous problems of minimum time orbit transfer and Solar System locally-optimal escape.

3.1 Minimum time orbit transfer

The first problem is to find the minimum time transfer trajectory between prescribed heliocentric coplanar orbits. Assuming an initial time $t_0 \triangleq 0$, the problem amounts to maximizing the performance index $J \triangleq -t_1$, where t_1 is the time at which the spacecraft reaches the target orbit.

Using Eq. (1) for the propulsive acceleration $\boldsymbol{a}$, the spacecraft dynamics is described by the following differential equations

$$\dot{r} = u \tag{9}$$

$$\dot{\nu} = v/r \tag{10}$$

$$\dot{u} = -\frac{\mu_\odot}{r^2} + \frac{v^2}{r} + \tau\, a_c \left(\frac{r_\oplus}{r}\right)^\eta C_D \tag{11}$$

$$\dot{v} = -\frac{u\, v}{r} + \tau\, a_c \left(\frac{r_\oplus}{r}\right)^\eta C_L \tag{12}$$

where u and v are the radial and circumferential components of the spacecraft velocity and $\mu_\odot$ is the Sun's gravitational parameter. The drag and lift coefficients C_D and C_L are given by Eqs. (2)-(3) as a function of the angle of attack θ.

Adopting an indirect approach, the Hamiltonian function associated to the problem is [31]

$$H \triangleq \lambda_r\, u + \frac{\lambda_\nu\, v}{r} + \lambda_u \left[-\frac{\mu_\odot}{r^2} + \frac{v^2}{r} + \tau\, a_c \left(\frac{r_\oplus}{r} \right)^\eta C_D \right] + \lambda_v \left[-\frac{u\, v}{r} + \tau\, a_c \left(\frac{r_\oplus}{r} \right)^\eta C_L \right] \tag{13}$$

where λ_i is the adjoint to i-th state variable. The Euler-Lagrange equations are

$$\dot{\lambda}_r = -\frac{\partial H}{\partial r} = \frac{\lambda_\nu\, v}{r^2} - \frac{2\,\lambda_u\,\mu_\odot}{r^3} + \frac{\lambda_u\, v^2}{r^2} - \frac{\lambda_v\, u\, v}{r^2} + \tau\,\eta\, a_c\, \frac{r_\oplus^\eta}{r^{\eta+1}} \left(\lambda_u\, C_D + \lambda_v\, C_L \right) \tag{14}$$

$$\dot{\lambda}_\nu = -\frac{\partial H}{\partial \nu} = 0 \tag{15}$$

$$\dot{\lambda}_u = -\frac{\partial H}{\partial u} = -\lambda_r + \frac{\lambda_v\, v}{r} \tag{16}$$

$$\dot{\lambda}_v = -\frac{\partial H}{\partial v} = \frac{\lambda_v\, u - 2\,\lambda_u\, v - \lambda_\nu}{r} \tag{17}$$

Equation (13) may be conveniently rewritten as

$$H = H' + \lambda_r\, u + \frac{\lambda_\nu\, v}{r} + \lambda_u \left(-\frac{\mu_\odot}{r^2} + \frac{v^2}{r} \right) - \lambda_v\, \frac{u\, v}{r} \tag{18}$$

where

$$H' = \tau\, a_c \left(\frac{r_\oplus}{r} \right)^\eta \sqrt{\lambda_u^2 + \lambda_v^2} \left(\frac{\lambda_u}{\sqrt{\lambda_u^2 + \lambda_v^2}}\, C_D + \frac{\lambda_v}{\sqrt{\lambda_u^2 + \lambda_v^2}}\, C_L \right) \tag{19}$$

is that portion of the Hamiltonian that explicitly depends on the two control variables, τ and θ.

From Pontryagin's maximum principle, the control variables must be chosen such that, at any time, the Hamiltonian is an absolute maximum. This amounts to maximizing H' with respect to τ and θ. Note that H' coincides with the expression $\boldsymbol{a} \cdot \boldsymbol{p}$ given by Eq. (5) provided that

$$\boldsymbol{p} = \lambda_u\, \hat{\boldsymbol{i}}_r + \lambda_v\, \hat{\boldsymbol{i}}_\nu \tag{20}$$

In other terms the optimal control law coincides with that drawn in Fig. 5 if

$$\cos\delta = \frac{\lambda_u}{\sqrt{\lambda_u^2 + \lambda_v^2}} \qquad , \qquad \sin\delta = \frac{\lambda_v}{\sqrt{\lambda_u^2 + \lambda_v^2}} \tag{21}$$

The vector $\boldsymbol{p}$ of Eq. (20) coincides, in this case, with the well known Lawden's primer vector [32].

3.2 Locally-optimal Solar System escape

A minimum time Solar System escape trajectory [33] may be conveniently approximated [34,35] by maximizing the instantaneous rate of change of the specific mechanical energy of the spacecraft $\mathcal{E} \triangleq (u^2+v^2)/2 - \mu_\odot/r$. Using the equations of motion (9)–(12) it may be shown that

$$\dot{\mathcal{E}} = \tau\, a_c \left(\frac{r_\oplus}{r}\right)^\eta \sqrt{u^2+v^2}\, \left(\frac{u}{\sqrt{u^2+v^2}}\, C_D + \frac{v}{\sqrt{u^2+v^2}}\, C_L\right) \tag{22}$$

which coincides with $\boldsymbol{a}\cdot\boldsymbol{p}$ provided that

$$\boldsymbol{p} = u\,\hat{\boldsymbol{i}}_r + v\,\hat{\boldsymbol{i}}_\nu \tag{23}$$

Therefore $\boldsymbol{p}$ now represents the spacecraft velocity vector. As in the previous problem, the optimal control law is drawn in Fig. 5 where

$$\cos\delta = \frac{u}{\sqrt{u^2+v^2}} \qquad , \qquad \sin\delta = \frac{v}{\sqrt{u^2+v^2}} \tag{24}$$

4 Numerical Examples

The previously discussed control laws are used to simulate optimal trajectories for a Magsail-based spacecraft in two mission scenarios.

4.1 Earth-Venus interplanetary transfer

As a first example, consider a circle-to-circle orbit transfer, starting from a parking orbit of radius $r = r_\oplus = 1\,\mathrm{AU}$. This situation corresponds to a heliocentric transfer that follows an Earth escape with zero hyperbolic excess velocity with respect to the planet. The final orbit radius coincides with the mean radius of Venus' heliocentric orbit, that is, $r_1 = 0.7233\,\mathrm{AU}$ and the Magsail characteristic acceleration is assumed to be $a_c = 1\,\mathrm{mm/s^2}$.

The two-point boundary value problem associated to the optimal control problem is constituted by the four equations of motion (9)–(12) and the four Euler-Lagrange equations (14)–(17). The boundary conditions are

$$
\begin{aligned}
& r(t_0) = r_\oplus \quad , \quad \nu(t_0) = 0 \quad , \quad u(t_0) = 0 \quad , \qquad v(t_0) = \sqrt{\frac{\mu_\odot}{r_\oplus}} \\
& r(t_1) = r_1 \quad , \quad u(t_1) = 0 \quad , \qquad v(t_1) = \sqrt{\frac{\mu_\odot}{r_1}} \quad , \quad \lambda_\nu(t_1) = 0 \quad , \quad H(t_1) = 1
\end{aligned}
\tag{25}
$$

where the last two equations follow from the transversality condition [36,37]. In particular, according to Ref. [37], the (necessary but not sufficient) condition $H(t_1) = 1$ allows a solution to be found for the minimum flight time.

The simulation results are summarized in Table 2. Two mission scenarios have been studied, one in which coasting arcs are allowed ($\tau = \{0, 1\}$), and the second in which the propulsion system is constrained to remain switched on ($\tau \equiv 1$) for all the mission length. In the latter circumstance τ is not a control variable, and the optimal control law for θ is that drawn in Fig. 5 where the shaded regions are now deleted. Notably, the mission times for the two mission scenarios are not much different. Likewise, the heliocentric trajectories are similar, as is shown in Figs. 6(a) and 6(c). On the other hand, the optimal steering laws for θ are significantly different, see Figs. 6(b) and 6(d).

Figure 7 shows the optimal transfer trajectory and the corresponding steering law for case B. Even though the resulting trajectory is similar to that of case A, the control laws are significantly different. This is due to the fact that the maximum value of the propulsive acceleration is reached for different values of θ, see Fig. 3.

4.2 Solar System escape mission

The second mission example involves the study of a Solar System escape trajectory using a locally-optimal control law, which maximizes $\dot{\mathcal{E}}$. The escape trajectory is simulated by forward integrating the equations of motion (9)–(12), using the previously discussed steering law, until the escape condition $\mathcal{E} = 0$ is met.

Assume that the spacecraft is initially moving along a circular parking orbit of radius $r = r_\oplus$ and belonging to the ecliptic plane. For symmetry reasons the initial true anomaly $\nu(t_0)$ may be set equal to zero. Therefore, the four boundary conditions necessary to integrate the equations of motions are the first four of Eqs. (25).

The time interval t_1 necessary to reach the escape condition is drawn in Fig. 8 as a function of $a_c \in [3,\, 5]\,\mathrm{mm/s^2}$ for both cases A and B. For comparative purposes, truly optimal trajectories have been simulated using an indirect approach adapted from that discussed in Ref. [38]. The results of this analysis have shown that locally-optimal escape trajectories are significantly different from truly-optimal trajectories when the characteristic acceleration is less than $3\,\mathrm{mm/s^2}$. The latter is thus the minimum value of a_c reported in Fig. 8.

Note that for the selected range of variation of a_c the locally-optimal trajectories are characterized by $r > r_\oplus$ for all $t \in [t_0,\, t_1]$. A typical example of this trajectory class is illustrated in Fig. 9(a). The reason for the time differences between cases A and B is that the spacecraft performance is strongly affected by the value of η, which models the way with which the maximum propulsive acceleration varies as a function of the distance from the Sun.

Finally Fig. 9(b) shows the time histories of angle of attack θ, thrust angle ϕ, and flight path angle, equal to $\arctan(u/v)$, for case B and $a_c = 3\,\mathrm{mm/s^2}$. The figure also illustrates the specific mechanical energy normalized by its initial value. Note that in the terminal phase of

the trajectory the thrust angle is close to zero, that is, the propulsive acceleration is nearly radially directed. The shape of the locally-optimal trajectory for case A, when a characteristic acceleration of $a_c = 3\,\mathrm{mm/s^2}$ is selected, is not shown because it is similar to that illustrated in Fig. 9(a).

5 Conclusions

The propulsive acceleration of a Magsail has been described by means of a mathematical model that captures the complex interactions between the magnetic field generated by the sail and the solar wind, in a two-dimensional mission scenario. The drag and lift coefficient, which define the magnitude of the propulsive acceleration, have been expressed in an analytical form as a function of the sail's angle of attack. The model has enabled the definition of optimal and locally-optimal steering laws by means of an indirect approach, and these results are new in the literature regarding magnetic sails. In particular, the problem of minimum time transfer trajectory between prescribed heliocentric orbits and the problem of maximizing the instantaneous rate of change of the orbital specific mechanical energy have been solved. The structure of the steering law is the same for both problems. Numerical simulations involving a minimum time Earth-Venus circle-to-circle interplanetary transfer and a Solar System escape two-dimensional mission have been discussed, using the spacecraft characteristic acceleration as a performance parameter.

A natural extension of the results discussed in this paper should involve the development of a three-dimensional thrust model for a Magsail. Such a model would permit not only a thorough analysis of an interplanetary transfer, but would also guarantee an estimate of the Magsail performance for more advanced missions, such as those toward the Heliopause nose.

Acknowledgments

The authors acknowledge the valuable support and suggestions by Prof. Yoshihiro Kajimura from the Akashi National College of Technology (Hyogo, Japan), and by Prof. Kazuhisa Fujita from the Japan Aerospace Exploration Agency.

References

[1] D. G. Andrews, R. M. Zubrin, Use of magnetic sails for mars exploration missions, in: AIAA/ASME/SAE/ASEE 25th Joint Propulsion Conference, Monterey (CA), 1989, paper AIAA 89-2861.

[2] D. G. Andrews, R. M. Zubrin, Progress in magnetic sails, in: AIAA/SAE/ASME/ASEE 26th Joint Propulsion Conference, Orlando (FL), 1990, paper AIAA 90-2367.

[3] D. G. Andrews, R. M. Zubrin, Magnetic sails and interstellar travel, Journal of The British Interplanetary Society 43 (6) (1990) 265–272 .

[4] R. M. Zubrin, D. G. Andrews, Magnetic sails and interplanetary travel, Journal of Spacecraft and Rockets 28 (2) (1991) 197–203, doi: 10.2514/3.26230.

[5] R. M. Zubrin, The use of magnetic sails to escape from low earth orbit, in: AIAA/SAE/ASME/ASEE 27th Joint Propulsion Conference, Sacramento (CA), 1991, paper AIAA 91-3352.

[6] R. M. Winglee, J. Slough, T. Ziemba, A. Goodson, Mini-magnetospheric plasma propulsion: Tapping the energy of the solar wind for spacecraft propulsion, Journal of Geophysical Research 105 (A9) (2000) 21,067–21,078, doi: 10.1029/1999JA000334.

[7] R. M. Winglee, T. Ziemba, L. Giersch, P. Euripides, J. Slough, Simulation of mini-magnetospheric plasma propulsion (m2p2) in the laboratory and space, in: 39th AIAA/ASME/SAE/ASEE Joint Propulsion Conference and Exhibit, Huntsville, Alabama, 2003, paper AIAA 2003-5224.

[8] P. Janhunen, Electric sail for spacecraft propulsion, Journal of Propulsion and Power 20 (4) (2004) 763–764, doi: 10.2514/1.8580.

[9] P. Janhunen, A. Sandroos, Simulation study of solar wind push on a charged wire: Basis of solar wind electric sail propulsion, Annales Geophysicae 25 (3) (2007) 755–767, doi: 10.5194/angeo-25-755-2007.

[10] K. Fujita, Particle simulation of moderately-sized magnetic sails, Journal of Space Technology and Science 20 (2) (2004) 26–31 .

[11] H. Nishida, H. Ogawa, I. Funaki, K. Fujita, H. Yamakawa, Y. Nakayama, Two-dimensional magnetohydrodynamic simulation of a magnetic sail, Journal of Spacecraft and Rockets 43 (3) (2006) 667–672, doi: 10.2514/1.15717.

[12] I. Funaki, H. Kojima, H. Yamakawa, Y. Nakayama, Y. Shimizu, Laboratory experiment of plasma flow around magnetic sail, Astrophysics and Space Science 307 (1–3) (2007) 63–68, doi: 10.1007/s10509-006-9251-4.

[13] K. Ueno, I. Funaki, T. Kimura, H. Horisawa, H. Yamakawa, Thrust measurement of a pure magnetic sail using the parallelogram-pendulum method, Journal of Propulsion and Power 25 (2) (2009) 536–539, doi: 10.2514/1.39211.

[14] Y. Kajimura, H. Usui, I. Funaki, K. Ueno, M. Nunami, I. Shinohara, M. Nakamura, H. Yamakawa, Hybrid particle-in-cell simulations of magnetic sail in laboratory experiment, Journal of Propulsion and Power 26 (1) (2010) 159–166, doi: 10.2514/1.45096.

[15] Y. Ashida, I. Funaki, H. Yamakawa, Y. Kajimura, H. Kojima, Thrust evaluation of a magnetic sail by flux-tube model, Journal of Propulsion and Power 28 (3) (2012) 642–651, doi: 10.2514/1.B34332.

[16] Y. Kajimura, I. Funaki, M. Matsumoto, I. Shinohara, H. Usui, H. Yamakawa, Thrust and attitude evaluation of magnetic sail by three-dimensional hybrid particle-in-cell code, Journal of Propulsion and Power 28 (3) (2012) 652–663, doi: 10.2514/1.B34334.

[17] H. Nishida, I. Funaki, Analysis of thrust characteristics of a magnetic sail in magnetized solar wind, Journal of Propulsion and Power 28 (3) (2012) 636–641, doi: 10.2514/1.B34260.

[18] G. Mengali, A. A. Quarta, Optimal missions with mini-magnetospheric plasma propulsion, Journal of Guidance, Control, and Dynamics 29 (1) (2006) 209–212, doi: 10.2514/1.18169.

[19] G. Mengali, A. A. Quarta, Minimagnetospheric plasma propulsion for outer planet missions, Journal of Guidance, Control, and Dynamics 29 (5) (2006) 1239–1242, doi: 10.2514/1.21634.

[20] G. Mengali, A. A. Quarta, P. Janhunen, Electric sail performance analysis, Journal of Spacecraft and Rockets 45 (1) (2008) 122–129, doi: 10.2514/1.31769.

[21] G. Mengali, A. A. Quarta, P. Janhunen, Considerations of electric sailcraft trajectory design, Journal of the British Interplanetary Society 61 (2008) 326–329 .

[22] A. A. Quarta, G. Mengali, P. Janhunen, Optimal interplanetary rendezvous combining electric sail and high thrust propulsion system, Acta Astronautica 68 (5-6) (2011) 603–621, doi: 10.1016/j.actaastro.2010.01.024.

[23] H. Kojima, I. Funaki, Y. Shimizu, H. Yamakawa, S. Shinohara, Y. Nakayama, Experimental simulation of a plasma flow around magnetic sail, in: 29th International Electric Propulsion Conference, Princeton (NJ), 2005, paper IEPC-2005-107.

[24] C. R. McInnes, Solar Sailing: Technology, Dynamics and Mission Applications, Springer-Praxis Series in Space Science and Technology, Springer-Verlag, Berlin, 1999, pp. 13–14, ISBN: 1-852-33102-X.

[25] M. Macdonald, C. R. McInnes, Solar sail science mission applications and advancement, Advances in Space Research 48 (11) (2011) 1702–1716, doi: 10.1016/j.asr.2011.03.018.

[26] C. Circi, Mars and mercury missions using solar sails and solar electric propulsion, Journal of Guidance, Control, and Dynamics 27 (3) (2004) 496–498, doi: 10.2514/1.5425.

[27] Y. Kajimura, personal communication, September, 26 2012. (September, 26 2012).

[28] B. Dachwald, Minimum transfer times for nonperfectly reflecting solar sailcraft, Journal of Spacecraft and Rockets 41 (4) (2004) 693–695, doi: 10.2514/1.6279.

[29] B. Dachwald, G. Mengali, A. A. Quarta, M. Macdonald, Parametric model and optimal control of solar sails with optical degradation, Journal of Guidance, Control, and Dynamics 29 (5) (2006) 1170–1178, doi: 10.2514/1.20313.

[30] P. Janhunen, et al., Electric solar wind sail: Towards test missions, Review of Scientific Instruments 81 (11) (2010) 111301–1–111301–11, doi: 10.1063/1.3514548.

[31] A. Bolle, C. Circi, A hybrid, self-adjusting search algorithm for optimal space trajectory design, Advances in Space Research 50 (4) (2012) 471–488, doi: 10.1016/j.asr.2012.04.026.

[32] D. F. Lawden, Optimal Trajectories for Space Navigation, Butterworths, London, 1963, pp. 54–68.

[33] S. Pizzurro, C. Circi, Optimal trajectories for solar bow shock mission, Cosmic Research 50 (6) (2012) 459–465, doi: 10.1134/S0010952512060056.

[34] G. Mengali, A. A. Quarta, Earth escape by ideal sail and solar-photon thrustor spacecraft, Journal of Guidance, Control, and Dynamics 27 (6) (2004) 1105–1108 .

[35] V. L. Coverstone, J. E. Prussing, Technique for escape from geosynchronous transfer orbit using a solar sail, Journal of Guidance, Control, and Dynamics 26 (4) (2003) 628–634 .

[36] A. E. Bryson, Y. C. Ho, Applied Optimal Control, Hemisphere Publishing Corporation, New York, NY, 1975, Ch. 2, pp. 71–89, ISBN: 0-891-16228-3.

[37] L. J. Wood, T. P. Bauer, Z. K. P., Comment on "time-optimal orbit transfer trajectory for solar sail spacecraft", Journal of Guidance, Control, and Dynamics 5 (2) (1982) 221–224, doi: 10.2514/3.56160.

[38] A. A. Quarta, G. Mengali, Electric sail mission analysis for outer solar system exploration, Journal of Guidance, Control, and Dynamics 33 (3) (2010) 740–755, doi: 10.2514/1.47006.

List of Tables

coefficient	case A	case B
h_0	0.8133	0.8312
h_1	0.1867	-0.1688
k_0	0.1485	-0.1338
k_1	0	-0.03969
η	2	4/3

Table 1
Best fit coefficients and thrust coefficient η, see Eqs. (1)–(3).

thrust model		t_1 [days]
	$\tau = 1$	378.2
case A		
	$\tau = \{0, 1\}$	374.3
	$\tau = 1$	386
case B		
	$\tau = \{0, 1\}$	372.8

Table 2
Earth-Venus (circle-to-circle) minimum transfer time for a_c=1mm/s^2.

List of Figures

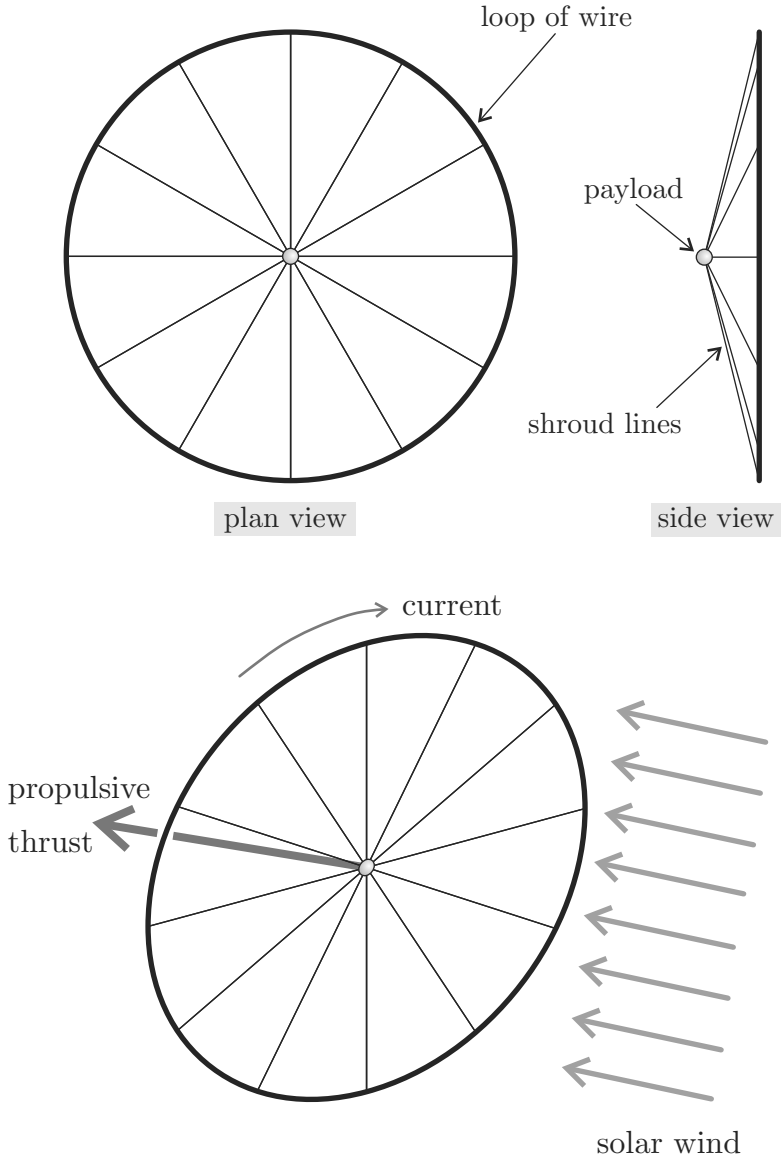

Figure 1. Magnetic sail schematic view (partially adapted from Ref. [4]).

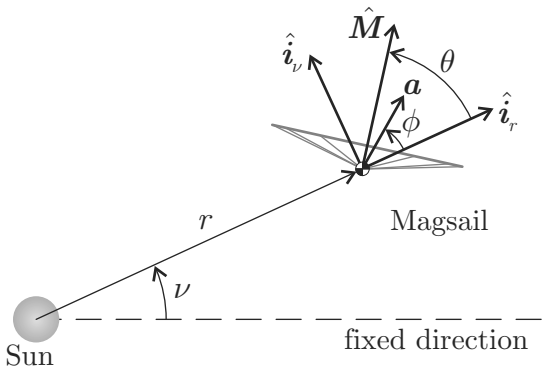

Figure 2. Reference frame and characteristic angles.

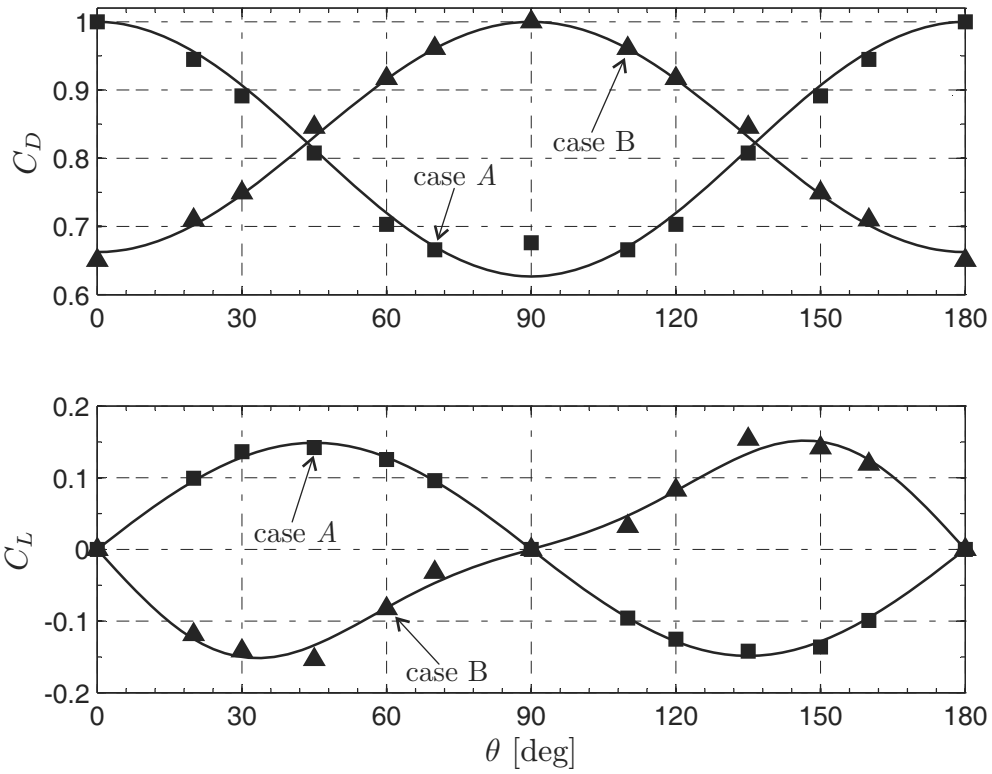

Figure 3. Lift and drag (normalized) coefficients as a function of θ (numerical data adapted from Ref. [16]).

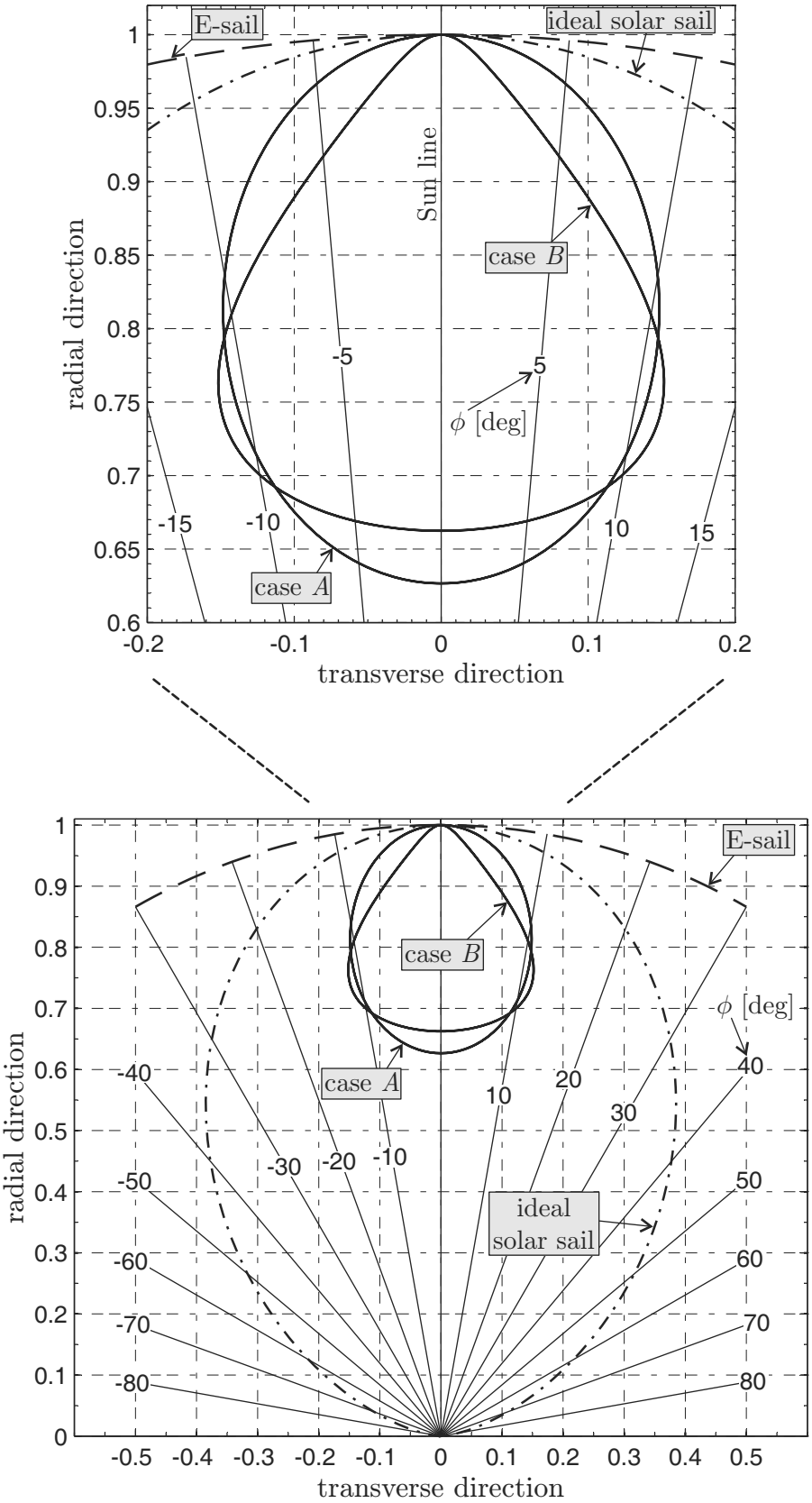

Figure 4. Diagram of the normalized propulsive acceleration vector endpoint for a Magsail, an E-sail, and a photonic (ideal) solar sail.

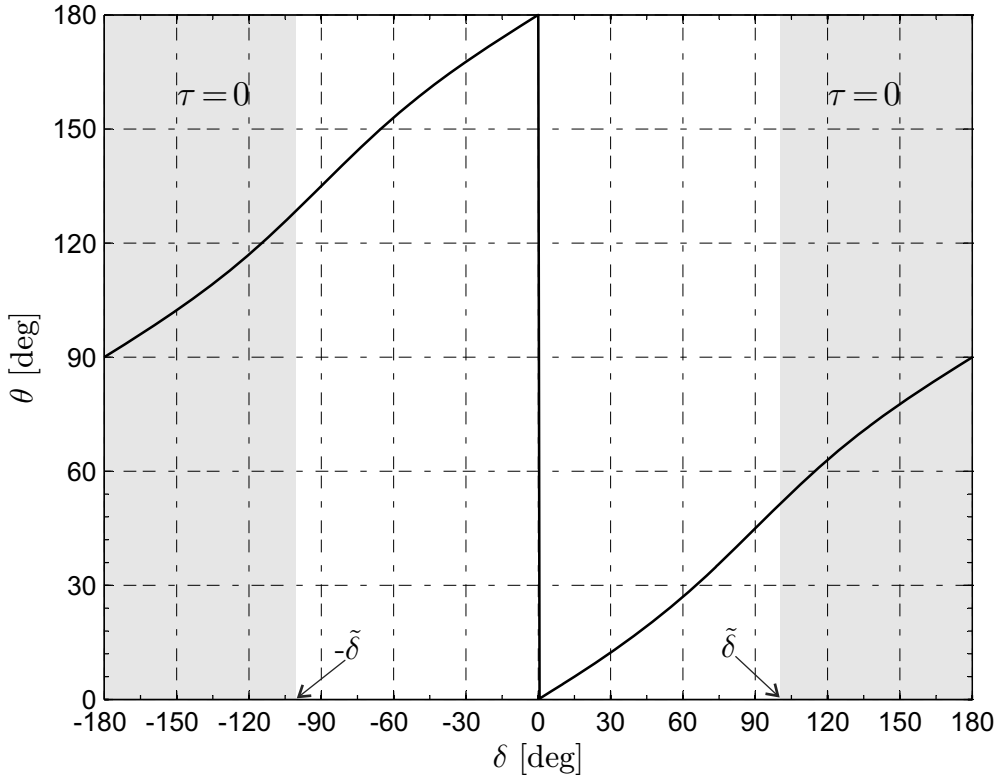

(a) case A.

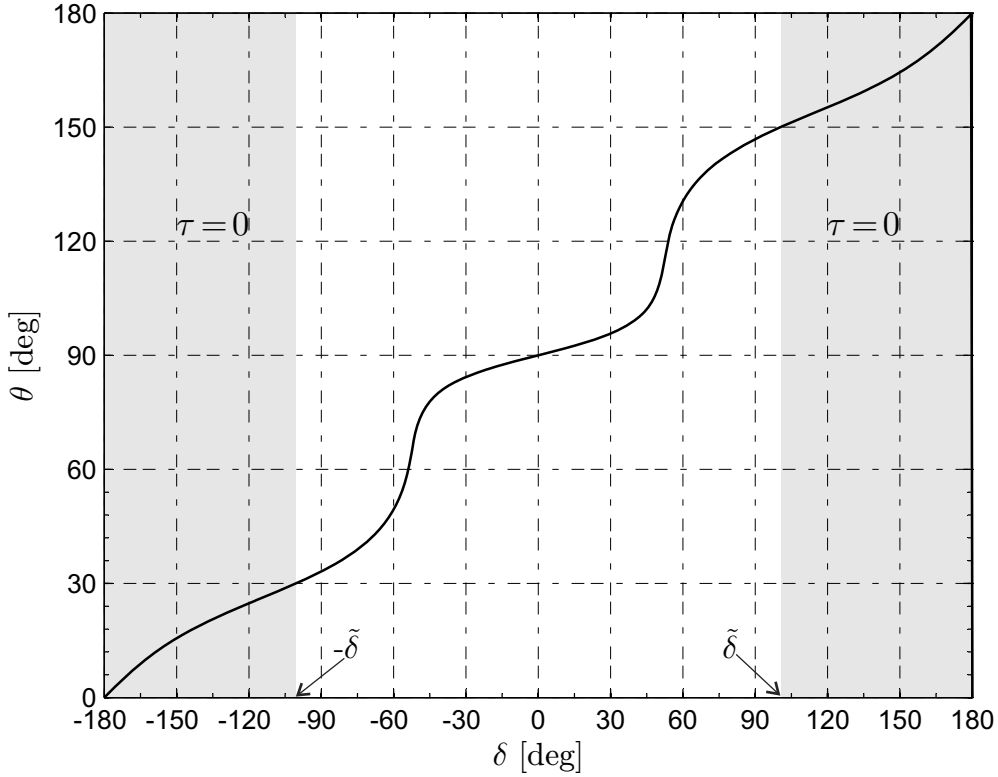

(b) case B.

Figure 5. Optimal angle of attack θ as a function of angle δ.

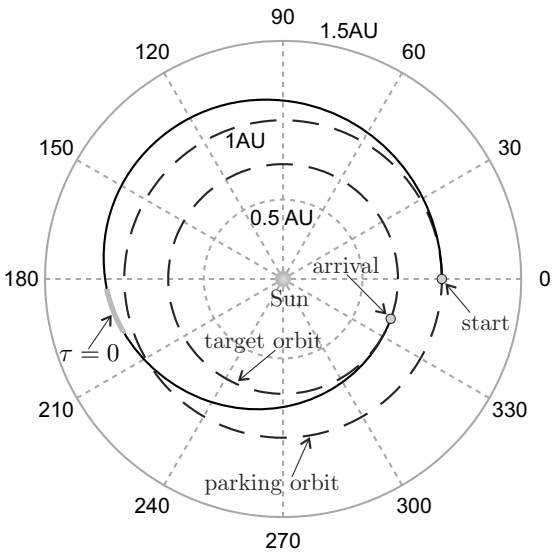

(a) Optimal trajectory ($\tau = \{0, 1\}$).

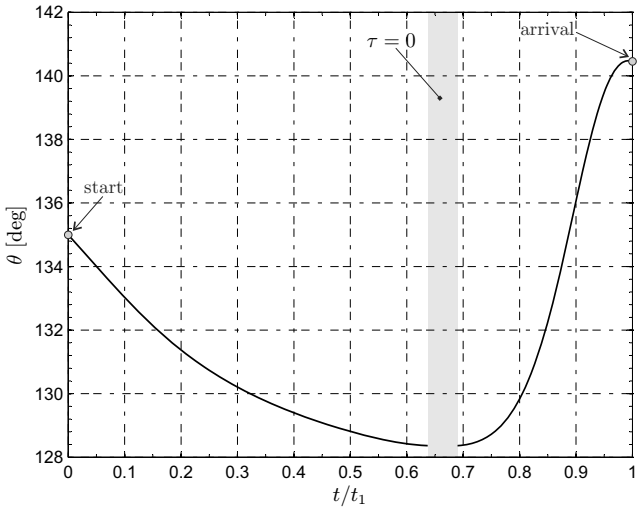

(b) Optimal control laws ($\tau = \{0, 1\}$).

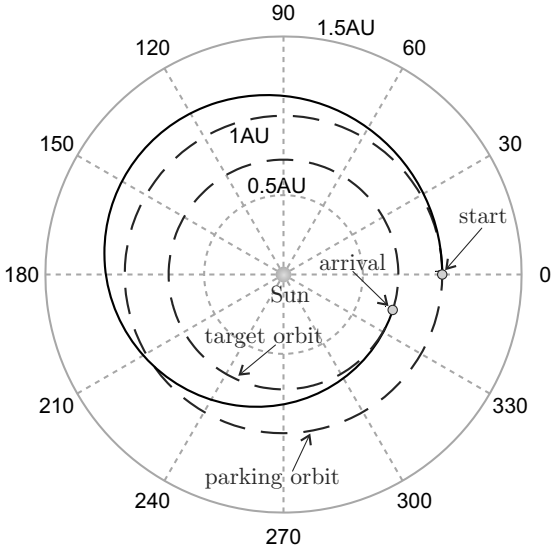

(c) Optimal trajectory ($\tau = 1$).

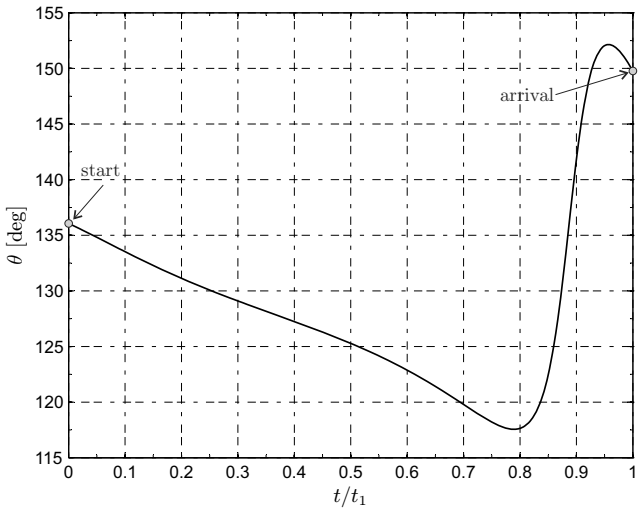

(d) Optimal control laws ($\tau = 1$).

Figure 6. Numerical example of Earth-Venus optimal transfer for case A, with a_c=1mm/s^2 and the data of Table 1.

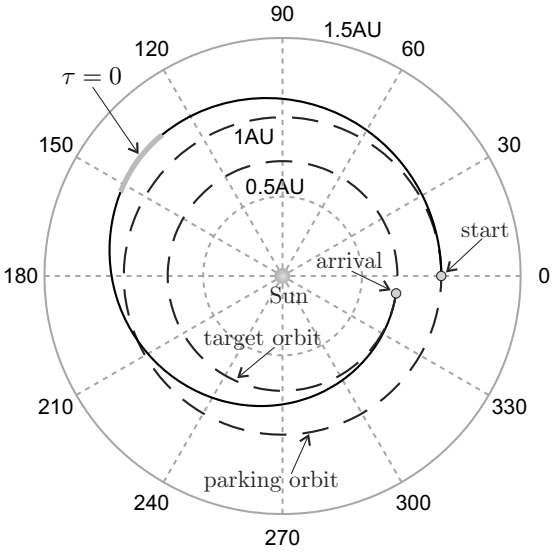

(a) Optimal trajectory ($\tau = \{0, 1\}$).

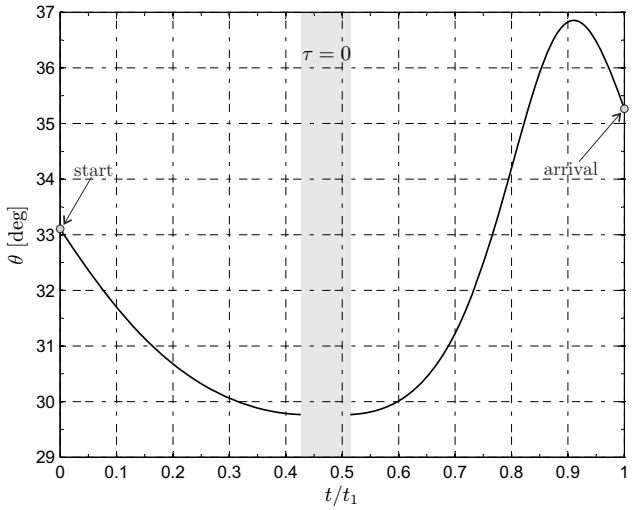

(b) Optimal control laws ($\tau = \{0, 1\}$).

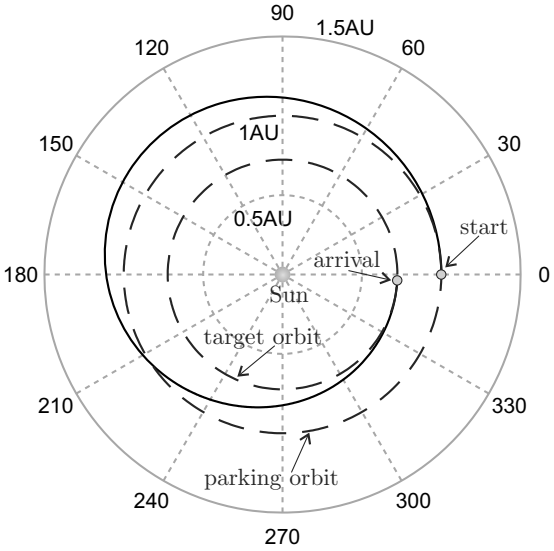

(c) Optimal trajectory ($\tau = 1$).

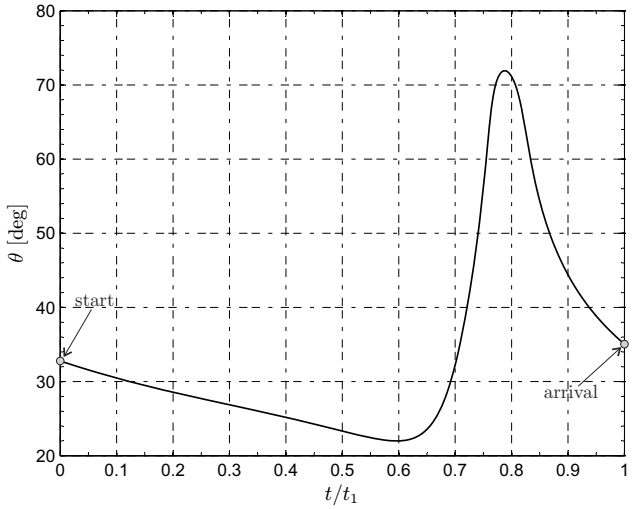

(d) Optimal control laws ($\tau = 1$).

Figure 7. Numerical example of Earth-Venus optimal transfer for case B, with a_c=1mm/s^2 and the data of Table 1.

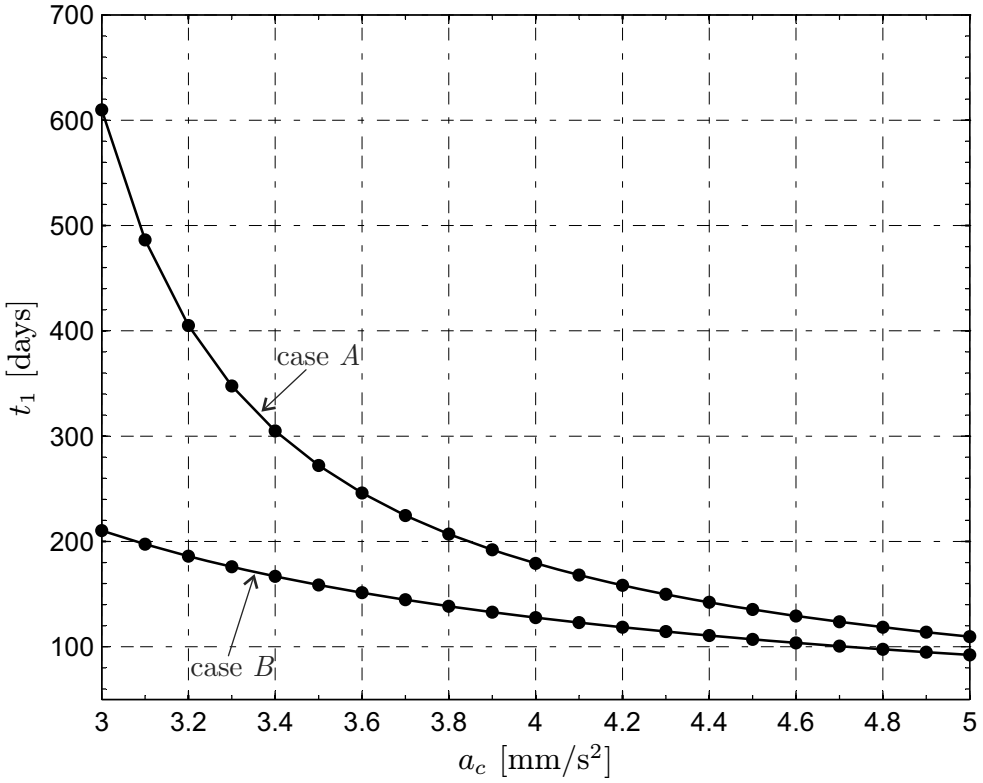

Figure 8. Flight time for Solar System escape using a locally-optimal control law and the data of Table 1.

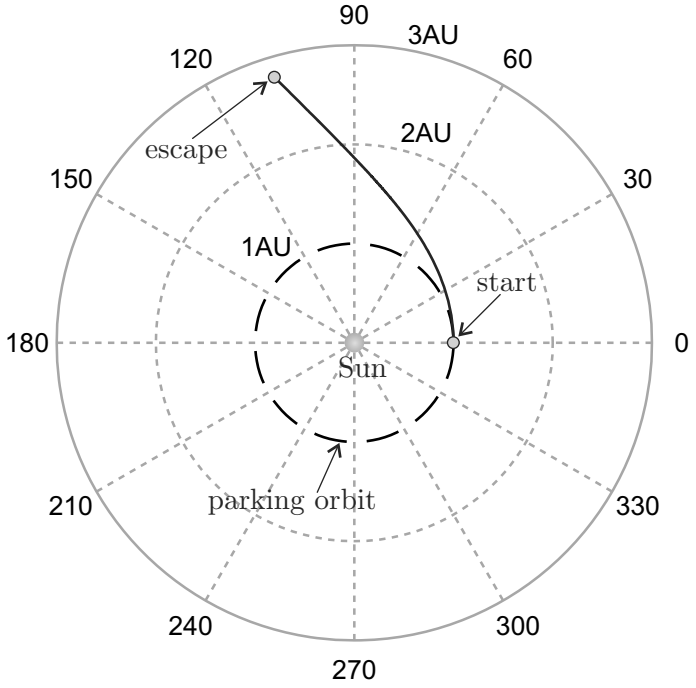

(a) Locally-optimal trajectory.

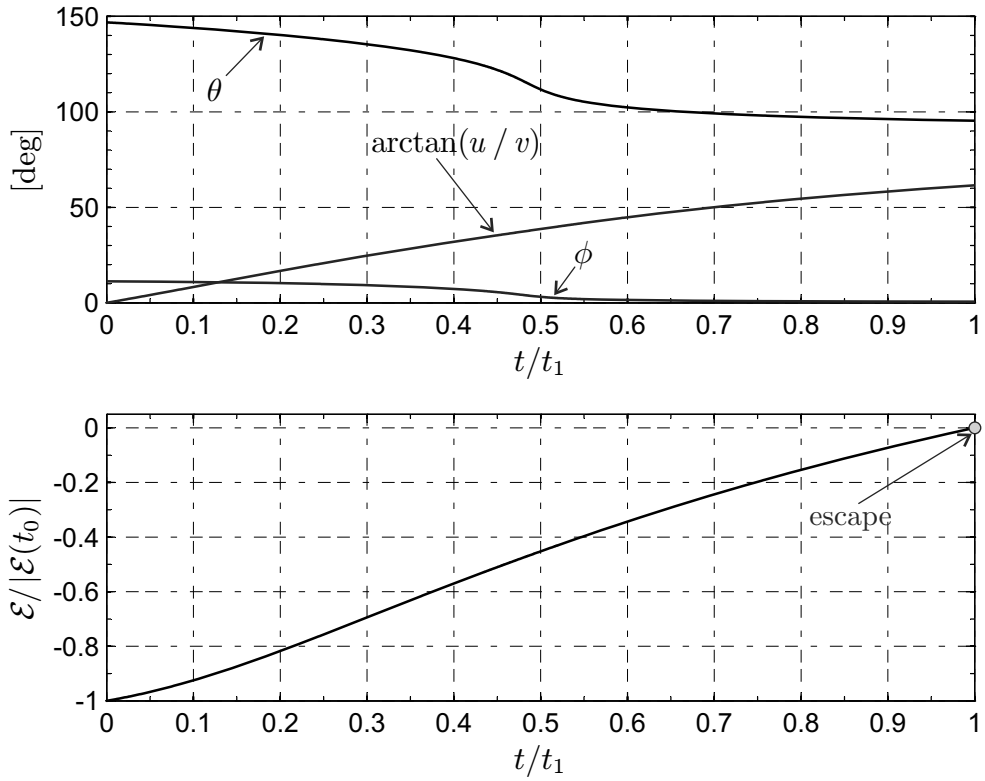

(b) Control angle and specific mechanical energy ($t_1 = 210$ days).

Figure 9. Results of a Solar System escape mission for case B, with $a_c = 3$ mm/s^2 and the data of Table 1.